REGULAR ARTICLE

Structural and electronic trends among group 15 polyhedral fullerenes

Antti J. Karttunen · Mikko Linnolahti ·
Tapani A. Pakkanen

Abstract We have investigated the structural and electronic characteristics of tetrahedral, octahedral, and icosahedral fullerenes composed of group 15 elements phosphorus, arsenic, antimony, and bismuth. Systematic quantum chemical studies at the DFT and MP2 levels of theory were performed to obtain periodic trends for the structural principles, stabilities, and electronic properties of the elemental nanostructures. Calibration calculations for polyhedral clusters with up to 20 atoms showed the applied theoretical approaches to be in good agreement with high-level CCSD(T)/cc-pVTZ results. By studying fullerenes up to P_{888}, As_{540}, Sb_{620}, and Bi_{620}, we found their structures and stabilities to converge smoothly toward their experimental bulk counterparts. The diameters of the largest studied cages were 4.8, 3.7, 4.8, and 5.1 nm for the P, As, Sb, and Bi fullerenes, respectively. Comparisons with the experimentally known allotropes of the studied elements suggest the predicted polyhedral cages to be thermodynamically stable. All studied group 15 polyhedral fullerenes were found to be semiconducting, and density of states analysis illustrated clear periodic trends in their electronic structure. Relativistic effects become increasingly important when moving from P to Bi and taking the spin–orbit effects into account by using a two-component

A. J. Karttunen (✉) · M. Linnolahti · T. A. Pakkanen
Department of Chemistry, University of Eastern Finland,
P.O. Box 111, 80101 Joensuu, Finland
e-mail: antti.j.karttunen@iki.fi
URL: http://www.uef.fi/modelling

procedure had a significant positive effect on the relative stability of bismuth clusters.

1 Introduction

Layered inorganic materials are a promising starting point for the synthesis of 1D and 0D nanostructures such as inorganic nanotubes and fullerenes. In addition to the appealing technological applications of the rich variety of inorganic fullerenes and nanotubes [1], the rationalization of their building principles provides insights into the fundamental structural chemistry of inorganic materials. Group 15 elements phosphorus, arsenic, antimony, and bismuth are all known to appear as layered materials composed of sheets of puckered six-membered rings, where the puckering is due to *p*-type lone pairs [2]. The layered bulk structures are structurally related to graphite, where the layers are composed of planar sheets of six-membered rings. In analogy to the structural relationship between the single layers of graphite and carbon fullerenes, the individual puckered sheets of the layered group 15 materials can be folded into fullerene-like polyhedral cages. In particular, we have recently demonstrated the structural feasibility of deriving polyhedral phosphorus fullerenes starting from the layered bulk structure [3].

Despite the close structural similarity of the layered bulk structures of group 15 elements, several notable periodic trends are apparent in the properties of group 15 elements when moving down from phosphorus to bismuth. From phosphorus to bismuth, the atomic number Z increases from 15 to 83, suggesting that relativistic effects play a key

role in the observed trends. The relativistic effects are particularly significant in the case of bismuth, where they are the root cause for the inertness of the 6 s electrons and the major spin–orbit effects that influence the chemistry of bismuth compounds [4, 5]. Concerning the electronic structure of the group 15 elements, two evident trends are the decrease in s–p mixing [6] and the increase in metallic character of the elements when moving from P to Bi. The decrease in s–p mixing has been suggested to explain why phosphorus prefers an orthorhombic bulk structure, while the heavier elements adopt a rhombohedral structure [6]. The increasing metallic character of the heavier elements is evident from their observed electronic properties: the orthorhombic black phosphorus is a semiconductor with a band gap of 0.33 eV [7, 8], but As, Sb, and Bi are all semimetals [9]. In addition to relativistic effects, the so-called secondary periodicity also affects the structural chemistry of group 15 elements [10]. In the case of arsenic, the electrons of the filled $3d$ shell shield the nucleus less efficiently in comparison with s and p electrons, leading into increase in the effective nuclear charge and an anomaly described as "d-block contraction". Analogous "lanthanoid contraction" also affects the properties of bismuth.

Polyhedral modifications of group 15 elements have been investigated in several studies previously, the smallest polyhedral cage, tetrahedron, being a well-known structural motif for group 15 elements. Solid P_4 (white phosphorus) and As_4 (yellow arsenic) have been known for a long time. Solid Sb_4 has been prepared and characterized very recently [11], while Bi_4 is currently known as a vapor-phase species. Larger polyhedral modifications have been investigated for all elements, as well. Icosahedral P_{20} was first studied by Häser et al. [12] who showed it to be unstable in comparison with P_4. Larger polyhedral phosphorus cages with up to 60 atoms have been predicted to be unstable with respect to dissociation into P_4 molecules, as well [13, 14]. In the case of arsenic, an I_h-symmetric $[As@Ni_{12}@As_{20}]^{3-}$ ion having As_{20} cage as its outer shell has been synthesized [15]. Theoretical studies on As_n cages up to $n = 20$ [16] and $n = 60$ [17] showed the dodecahedral As_{20} cage to be energetically comparable to As_4. Icosahedral, puckered arsenic cages have been investigated recently, and the single-layered, icosahedral arsenic cages were shown to be surpassed in stability by chain-like allotropes [18, 19]. In the case of antimony, Kumar has studied the small Sb_4 and Sb_8 cages. Experimental investigation into Sb clusters by means of mass spectrometry has revealed a large number of clearly resolved cluster compositions up to Sb_{100} following a sequence Sb_{4n}, while a completely different kind of size distribution of clusters was observed for bismuth [20]. For bismuth, various polyhedral modifications have been studied very recently.

Zdetsis investigated a family of bismuth fullerenes up to Bi_{80}, together with several fullerenes-like structures of P, As, and Sb. The puckered Bi_{80} fullerene was predicted to be the energetically most favorable, in agreement with previous studies for polyhedral phosphorus and arsenic fullerenes [21]. Bismuth cages up to Bi_{60} were also investigated in another recent theoretical study, but the small non-puckered clusters were found to be unstable with respect to collapsing into a dense cluster [22]. Polyhedral bismuth cages have also been prepared and characterized experimentally, an illustrative example being the highly symmetric $[Bi_{10}Au_2]^{6+}$ heteroicosahedron, which contains a pentagonal $[Bi_{10}]^{4+}$ antiprism capped by gold atoms [23].

In our recent systematic investigation into phosphorus fullerenes, we derived general structural principles of polyhedral phosphorus cages. The derived structural principles were expected to apply for the heavier group 15 congeners, as well [21]. Here, we carry out a quantum chemical study on polyhedral fullerenes composed of group 15 elements phosphorus, arsenic, antimony, and bismuth. The tetrahedral, octahedral, and icosahedral cages are systematically investigated, and their thermodynamic stabilities are compared with the experimentally known allotropic forms of the elements. In analogy to our recent study on the structural and electronic trends of nanotubular modifications of group 15 elements [24], we aim to shed light on various periodic trends for the structures composed of elements P–Bi. For the heavier elements Sb and Bi, we examine the impact of both scalar and spin–orbit relativistic effects on their stability and electronic structure.

2 Computational details

The group 15 polyhedral fullerenes were investigated by using the BP86 density functional [25–27] and ab initio MP2 methods. The Karlsruhe split-valence basis set with polarization functions (def2-SVP) was applied for all atoms in the BP86 calculations [28, 29], and the Karlsruhe triple-valence-zeta basis set with polarization functions was used in the MP2 calculations (P, As: def-TZVP; Sb, Bi: def2-TZVP) [29, 30]. 28-electron and 60-electron scalar relativistic effective core potentials (ECP) were used to describe the core electrons of antimony and bismuth, respectively [31]. Resolution-of-the-identity (RI) technique was used to speed up both DFT [32–35] and MP2 [36–40] calculations. All structures were fully optimized within their respective point group symmetries using the BP86 method. Single-point MP2 calculations with frozen core orbitals were made at the BP86-optimized geometries (P: $1s2s2p$; As: $1s2s2p3s3p$; Sb: ECP + $4s4p$; Bi: ECP + $5s5p$).

We evaluated the accuracy of the BP86/SVP and MP2/TZVP levels of theory by comparing the relative energies of small phosphorus and arsenic clusters to relative energies obtained at the CCSD(T)/cc-pVTZ [41, 42] level of theory. The phosphorus $1s2s2p$ and arsenic $1s2s2p3s3p$ core orbitals were frozen in the CCSD(T) calculations. The results of the comparison are shown in Fig. 1. The relative energy trends of the polyhedral clusters predicted by the BP86/SVP and MP2/TZVP levels are in good agreement with the results obtained at the CCSD(T)/cc-pVTZ level. In particular, the MP2/TZVP results are in excellent agreement with the relative CCSD(T)/cc-pVTZ energies for M_{12}, M_{16}, and M_{20} (M = P, As).

BP86/SVP vibrational frequency calculations were made for polyhedra up to P_{344}, As_{200}, Sb_{248}, and Bi_{248} to verify them as true local minima and to obtain Gibbs free energies [43]. MP2 Gibbs free energies were calculated by using Gibbs corrections obtained at the BP86/SVP level of theory. DFT and MP2 calculations were made using TURBOMOLE (versions 5.9.1 and 5.10) [44]. Spin–orbit effects for antimony and bismuth clusters were investigated at the BP86/def2-TZVP-2c level of theory using the efficient two-component procedure implemented in TURBOMOLE (core electrons were described with scalar

relativistic ECPs) [45]. CCSD(T) calculations were made with the CFOUR program package [46, 47]. The relative energies of the infinite monolayer sheets of the rhombohedral crystal structures were estimated using an extrapolation scheme calibrated against true periodic calculations (see Ref. [3] for details).

3 Results and discussion

3.1 Structural principles of the studied fullerenes

The structural principles of the studied polyhedral group 15 fullerenes have been described in detail in our previous study on polyhedral phosphorus cages [21]. Therefore, we only summarize their most important structural characteristics here. The studied polyhedral group 15 fullerenes are structurally related to the layered, rhombohedral bulk materials (Fig. 2a, b). The regular polyhedra are composed of triangular faces, which can be considered as finite pieces cut from a monolayer sheet of the rhombohedral bulk. We focus on three distinct structural families, tetrahedra, octahedra, and icosahedra, each of which contains an infinite number of members. The structures have been classified using a systematic scheme similar to that previously used for carbon fullerenes [48, 49]. In the applied scheme, each polyhedral cage is uniquely defined by a lattice vector (h,k) describing how the triangular faces of the cage are cut from a monolayer sheet of rhombohedral bulk (Fig. 2c). The resulting polyhedra are composed of six-membered rings, with their vertices being capped with three-, four- or five-membered rings in the case of tetrahedral, octahedral, or icosahedral fullerenes, respectively (Fig. 2d). The number of atoms in each polyhedron depends on (1) the topology of the cage (that is, total number of triangular faces) and (2) the lattice vector (h,k), resulting in the following formulas for the number of atoms tetrahedral, octahedral, and icosahedral cages, respectively, $4(h^2 + hk + k^2)$, $8(h^2 + hk + k^2)$, and $20(h^2 + hk + k^2)$ [21]. In analogy to the naming conventions of carbon nanotubes [50], the members of the $(h,0)$ and (h,h) structural series can be considered as zigzag and armchair cages, all the other cages being chiral. Notably, the puckered structure of the triangular faces of the cages gives rise to structural "in–out" isomerism [51–53], where each nonvertex atom can in principle point either outwards or inwards (that is, toward the cage center). We have taken this isomerism into account by systematically investigating the different symmetry-allowed structural isomers to find out the most favorable configuration for each (h,k) structural series (for details, see ref. [21]).

Concerning the energetic of the polyhedral fullerenes, folding a monolayer sheet of rhombohedral bulk into a
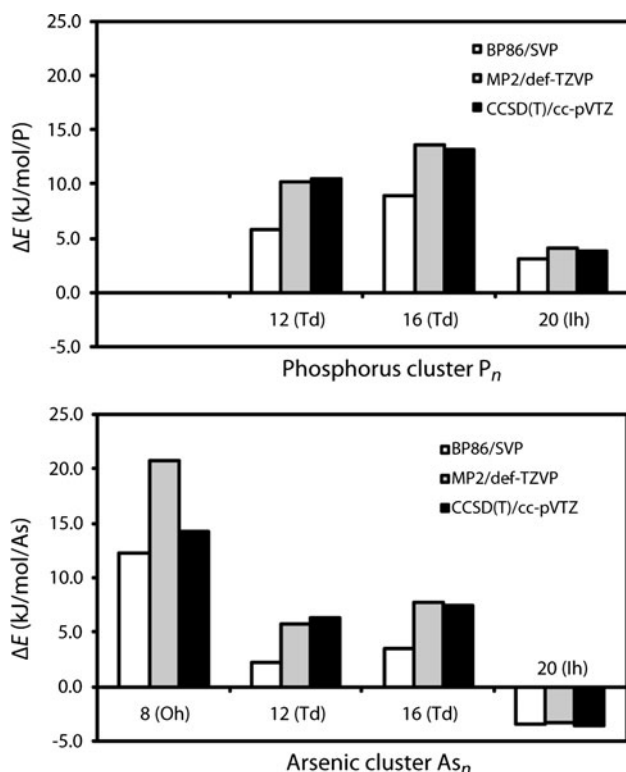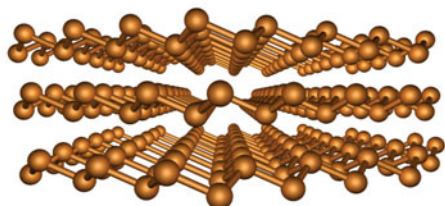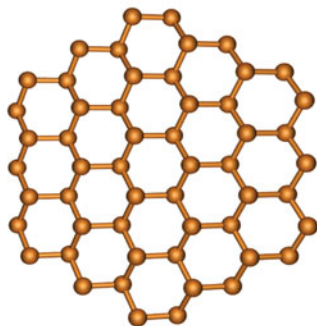

Fig. 1 Relative energies of several phosphorus and arsenic clusters calculated at different levels of theory. BP86/SVP geometries were applied in all cases. The energies are given relative to the experimentally known tetrahedral P_4 and As_4 cages. The P_8 cage has been omitted, because it is not a true local minimum structure
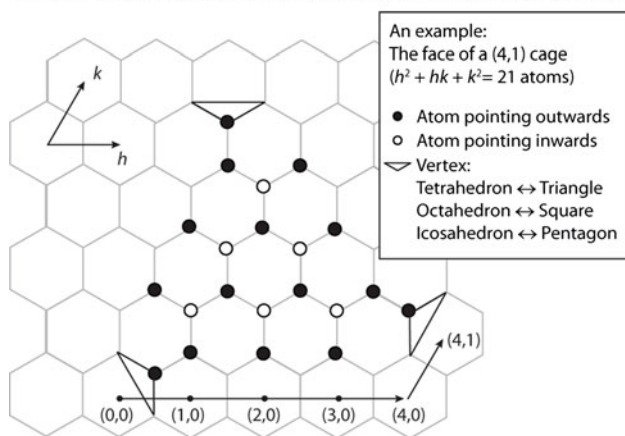
a A side view of the rhombohedral crystal structure of the group 15 elements (the most stable form for As, Sb, and Bi, a high-pressure modification for P)

b A top view of a monolayer sheet of the rhomcohedral crystal structure

c The lattice vector (h,k) defines how the face of a polyhedron is constructed from a network of hexagonal rings, that is, the rhombohedral monolayer sheet

An example:
The face of a (4,1) cage
($h^2 + hk + k^2 = 21$ atoms)

● Atom pointing outwards
○ Atom pointing inwards
▽ Vertex:
Tetrahedron ↔ Triangle
Octahedron ↔ Square
Icosahedron ↔ Pentagon

d Three polyhedral cages resulting from the (4,1) face configuration. The equivalent faces are colored with darker shade.

Tetrahedral (4,1) cage
($4 \times 21 = 84$ atoms)

Octahedral (4,1) cage
($8 \times 21 = 168$ atoms)

Icosahedral (4,1) cage
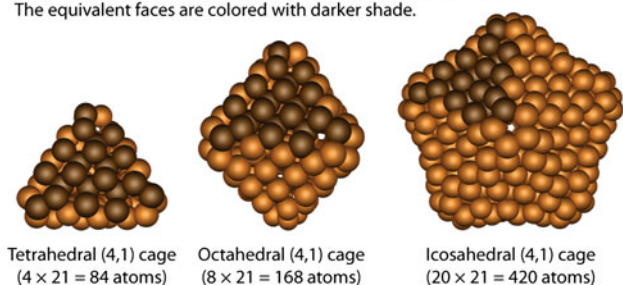($20 \times 21 = 420$ atoms)

Fig. 2 The structural principles of the group 15 polyhedral fullerenes

polyhedron gives rise to structural strain due to the vertices and edges adjoining the triangular faces. This is because the coordination of the vertex and edge atoms deviates from the optimal chair conformation of the six-membered rings present in the monolayer sheet of the rhombohedral
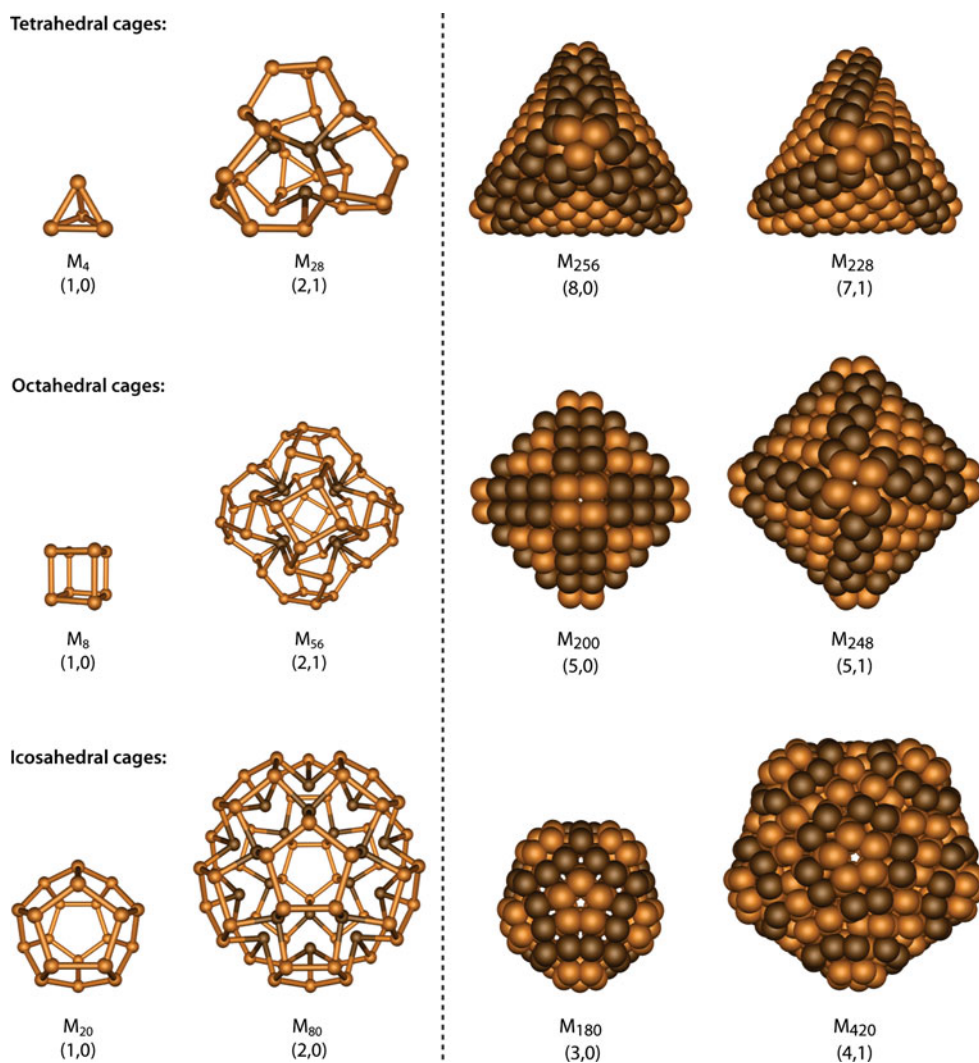
bulk. In practice, the deviations from the chair conformation result in less favorable bond lengths and angles, together with increased lone pair repulsion. Generally, the most favorable structural isomer of any cage results from maximizing the number of atoms with coordination similar to rhombohedral bulk, thus minimizing the structural strain resulting from vertices and edges.

Before moving on to the computational results in the next chapter, we discuss few illustrative structural examples from each polyhedral family at a qualitative level in order to elucidate their structural characteristics. Starting from the tetrahedral family, the smallest possible structure $[(h,k) = (1,0)]$ is the experimentally well-known species, tetrahedron (M_4, Fig. 3). The two next members of the tetrahedral family, M_{12} (1,1) and M_{16}, (2,0), have been discussed in more detail previously [21], and we focus on the fourth largest tetrahedral cage, M_{28} (2,1), which is large enough to display the "in–out isomerism" that is of fundamental importance to the group 15 fullerenes (Fig. 3). In M_{28}, every other atom at the distance of two M–M bonds from each vertex atom can point inwards, allowing the six-membered rings to pucker. From the onset of this "in–out" isomerism, the larger cages become increasingly stable, as their facets start to approach structurally the puckered monolayer sheet of the rhombohedral bulk. The M_{228} (7,1) and M_{256} (8,0) structures in Fig. 3 are examples of large tetrahedral cages, where the planar triangular facets are clearly visible. The M_{228} (7,1) cage also illustrates the relatively favorable coordination of the edge atoms, which is present in all members of the (h,1) structural series. This structural feature makes the tetrahedral (h,1) cages favored over the other structural series such as (h,0), (h,2), or (h,h) [21].

In the case of the octahedral structures, the smallest polyhedron is the M_8 cube and the first puckered "in–out" cage feasible for all group 15 elements is the M_{56} cage, also with (h,k) lattice vector (2,1) in analogy to the tetrahedral structures (Fig. 3). The M_{200} (5,0) and M_{248} (5,1) cages illustrate the structural characteristics of larger octahedral cages. As for the tetrahedral structures, the favorable coordination of the edge atoms in the octahedral (h,1) cages reduces the structural strain. However, for the octahedral (h,0) structures, the strain due to edge atoms is also reduced significantly in comparison with their tetrahedral counterparts [21].

The smallest icosahedral structure is the M_{20} dodecahedron, the first puckered cage being the M_{80} cage (Fig. 3). In contrast to the tetrahedra and octahedra, the icosahedral (h,0) series are favored over the icosahedral (h,1) series due to the large number of vertices in the icosahedra [21]. Although the coordination of the edge atoms is not optimal in the favored (h,0) cages, the less strained arrangement of the vertex atoms compensates for this drawback [21].

Fig. 3 Illustrative examples of the group 15 polyhedral fullerenes. *Left* The smallest [$(h,k) = (1,0)$] polyhedral cage of each structural family, together with the smallest cage where the in–out isomerism becomes energetically favorable (the atoms pointing toward the interior of the cages are colored with *darker shade*). *Right* Examples of the larger polyhedral structures drawn as space-filling models (non-vertex atoms with coordination different from a rhombohedral sheet are colored with *darker shade*)

Tetrahedral cages:

M_4 (1,0) M_{28} (2,1) M_{256} (8,0) M_{228} (7,1)

Octahedral cages:

M_8 (1,0) M_{56} (2,1) M_{200} (5,0) M_{248} (5,1)

Icosahedral cages:

M_{20} (1,0) M_{80} (2,0) M_{180} (3,0) M_{420} (4,1)
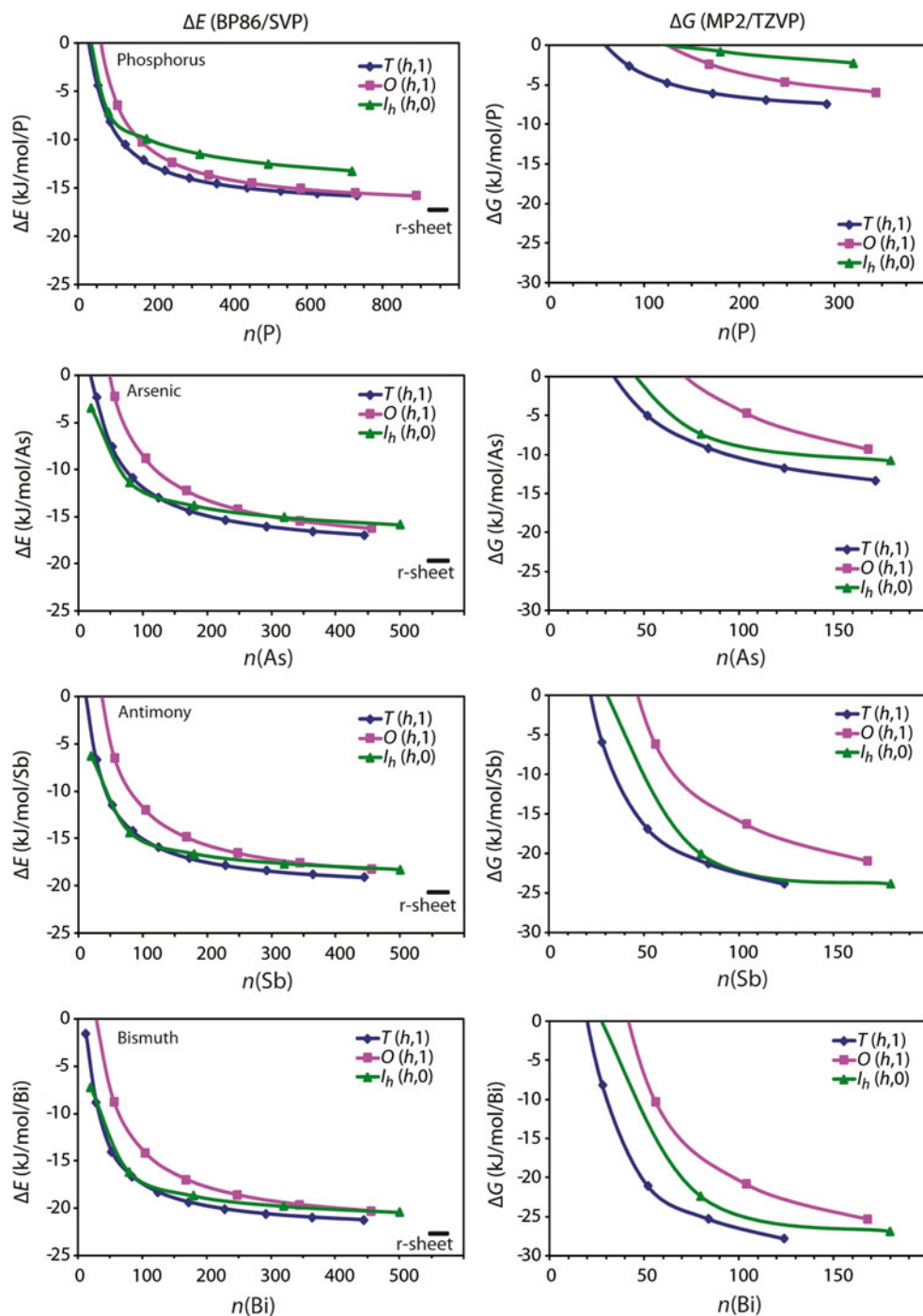
3.2 Energetic and thermodynamic trends

We studied P, As, Sb, and Bi fullerenes up to P_{888}, As_{540}, Sb_{620}, and Bi_{620} to shed light on the structural trends among them. The diameters of the largest studied cages were 4.8, 3.7, 4.8, and 5.1 nm for the P, As, Sb, and Bi, respectively. In terms of lattice vector (h,k), the largest studied cages were the tetrahedral (13,1), octahedral (10,1), and icosahedral (6,1) structures composed of phosphorus. The relative energies of the fullerenes were determined by comparing them with the experimentally known tetrahedral four-atomic species, which is also the smallest possible polyhedron. We also considered the stabilities of the fullerenes with respect to corresponding infinite monolayer sheet of rhombohedral bulk, which can be considered as a strain-free reference structure.

The energetic and thermodynamic trends of the studied fullerenes are shown in Fig. 4. The BP86 and MP2 levels of theory predict similar stability trends. Overall, as the structures become larger, all three studied structural families of group 15 fullerenes approach the monolayer sheet of the rhombohedral bulk in energy. A notable periodic trend is that the polyhedral group 15 fullerenes become less strained with respect to the monolayer sheet of the rhombohedral bulk when moving down from P to Bi. For example, the strain energies calculated for the tetrahedral M_{444} (10,1) cage are 2.3, 2.5, 1.6, and 1.4 kJ/mol/atom for P, As, Sb, and Bi, respectively. The obtained strain energies of a few kJ/mol/atom for the largest studied cages can be considered as very small. For comparison, the strain energy of a C_{60} fullerene with respect to a graphene sheet is about 40 kJ mol^{-1} per atom at a similar level of theory [54].

Overall, the tetrahedral structures were found to be the thermodynamically most favorable for all elements, and for all elements, the smallest polyhedron with $\Delta G < 0$ also belongs to the tetrahedral structural family: P_{84} (−2.7 kJ/mol/P), As_{52} (−5.0 kJ/mol/As), Sb_{28} (−5.9 kJ/ml/Sb), and Bi_{28} (−8.1 kJ/mol/atom). The larger octahedral and icosahedral structures are also thermodynamically stable with

Fig. 4 Relative BP86/SVP total energies and MP2/TZVP Gibbs free energies of the favored structural series of group 15 polyhedra ($T = 298.15$ K, $p = 0.1$ MPa). The energies and free energies are given relative to the experimentally known tetrahedral M$_4$ cages. The value at *r-sheet* denotes the relative energy of an infinite rhombohedral monolayer sheet (see Fig. 1)

respect to M$_4$ tetrahedral structures, and for As, Sb, and Bi, the icosahedral structures are actually rather close to the tetrahedral structures in stability. For tetrahedral structures, the $(h,1)$ structural series is preferred for all elements due the favorable structural features discussed in the previous chapter. In the case of octahedral structures of heavier elements Sb and Bi, the large octahedral $(h,0)$ cages are energetically very close to the favoured $(h,1)$ structures (not shown in Fig. 4). Evidently, the structural strain due to

the edges in the $(h,0)$ structures is not that significant for Sb and Bi because of inherently longer M–M bond lengths. The more flexible pure p-type bonding might also play a role for here (see the discussion on the electronic structure in Sect. 3.4). For the icosahedral structures, the $(h,0)$ structural series is always favored over the other series for the cages studied here.

The cages can be further stabilized by multilayering, where smaller cages are embedded inside larger ones,

resulting structures that are very closely related to the layered bulk materials. We have previously demonstrated the energetic favorability of multilayered polyhedral cages such as the tetrahedral $P_{52}@P_{364}$ [3]. Multilayered 0D-structures would also be a reasonable outcome if the layered bulk materials are used as a starting point for synthesis. A direct approach for synthesis from bulk materials would be the arc discharge method used in the synthesis of graphitic carbon nanostructures [55]. Various other techniques have been used to produce group 15 clusters, as well. For example, laser ablation has been successfully used to produce phosphorus [56–59] and arsenic clusters [60]. In the case of the heavier group 15 elements, antimony and bismuth clusters have been prepared via nucleation from metal vapors [20]. However, the abovementioned techniques are inherently high-temperature methods, which might not be beneficial for the formation of large polyhedral cages. Interestingly, one-dimensional group 15 nanostructures, the experimentally known antimony and bismuth nanotubes, have been synthesized via low-temperature routes such as hydrothermal reduction methods [61]. Concerning the applications of group 15 nanostructures, the interest in the nanostructured modifications of antimony and bismuth arises from their unique electronic transport properties which suggest them to possess promising thermoelectric applications [62]. Phosphorus nanostructures also have attractive applications, the recently demonstrated applicability of layered bulk phosphorus as an anode material for Li-ion batteries suggesting that new anode materials based on nanostructured modifications of phosphorus could possess high application potential [63].

In addition to the studied hollow cages, there are other relevant structural isomers that might be favored over the cages within the size range investigated here. For example, for phosphorus and arsenic, ring-shaped clusters have been previously shown to be favored over the single-layered hollow cages of the same size [18, 19]. To shed light on the relative stabilities of the various isomers, we compared the studied hollow cages to a more compact, ring-shaped D_{6d}-symmetric M_{144} cluster that has been previously shown to be a thermodynamically favorable structural motif for phosphorus and arsenic [18, 19]. The ΔG_{MP2} in comparison with M_4 for P_{144}, As_{144}, Sb_{144}, and Bi_{144} are -8.7, -12.1, -15.2, and -14.6 kJ/mol/atom, respectively. The corresponding relative Gibbs free energies in comparison with the tetrahedral M_{124} cage in the same size domain are -3.9, -0.4, 8.7, and 13.2 kJ/mol/atom, respectively. In summary, in this size domain, the ring-shaped structures appear to be favored for P and As, while the cage-shaped structures are favored for Sb and Bi. This is understandable considering the known structural characteristics of the group 15 elements: for phosphorus and arsenic, the chain-like modifications structurally related to

the ring-shaped clusters have been synthesized as pure P structures [64] and P–As mixtures [65], but for antimony and bismuth such forms have not been observed to date. The present results for the ring-shaped Sb and Bi structures should be considered as preliminary examples, and detailed studies on the compact isomers of antimony and bismuth are expected to further elucidate the structural characteristics of allotropic modifications in the heavier group 15 elements. In the case of phosphorus and arsenic, the cage-shaped isomers might be attainable as multilayered species, in analogy to the layered bulk materials.

3.3 The impact of spin–orbit effects

As discussed in the computational details section, scalar relativistic effects were taken into account for the heavier group 15 elements, Sb and Bi, by means of effective core potentials. However, especially for Bi clusters, the spin–orbit effects can be very significant, as well. Therefore, we performed two-component calculations at the BP86/def2-TZVP-2c level of theory for Sb and Bi clusters with up to 24 atoms to investigate the impact of spin–orbit effects on their relative stabilities (Fig. 5). Extensive two-component
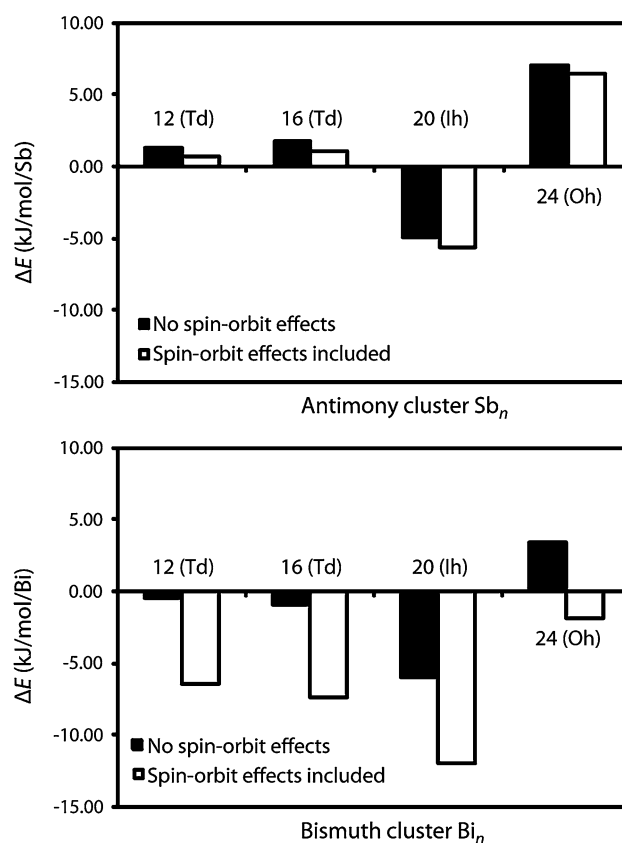

Fig. 5 The impact of spin–orbit effects for antimony and bismuth clusters with up to 24 atoms (all calculations done at the BP86/def2-TZVP-2c level of theory). The energies are given relative to the experimentally known tetrahedral M_4 cages
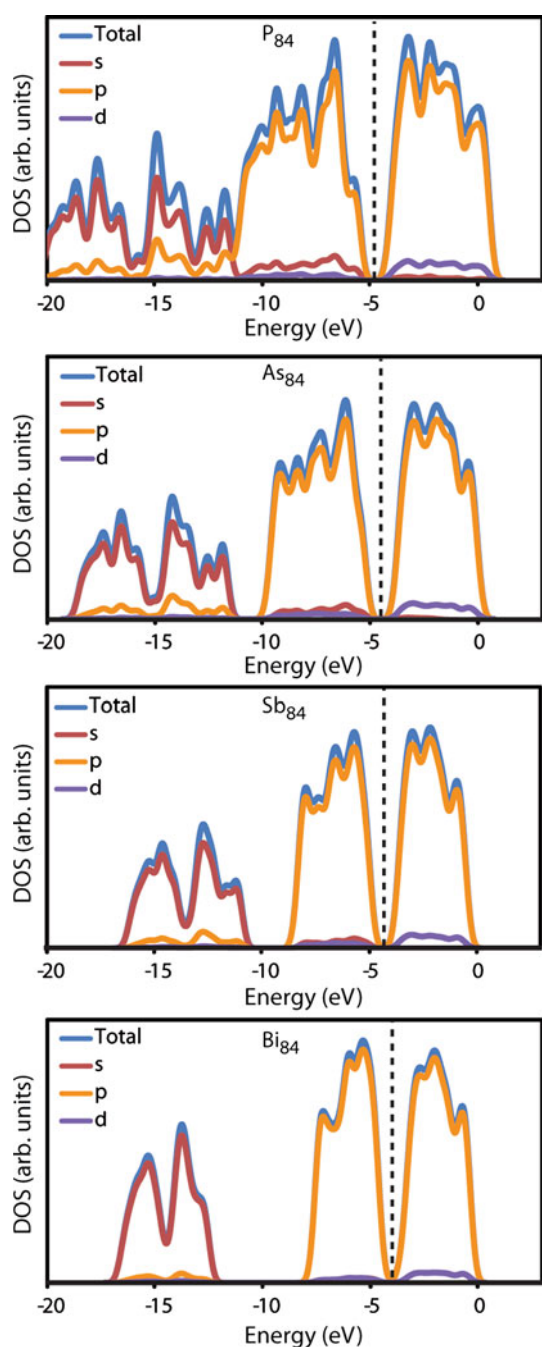
Fig. 6 Density of states (DOS) plots for the tetrahedral M_{84} cages. The *dotted lines* denote the HOMO-LUMO gaps

calculations on larger clusters were not feasible this time due to their significantly higher computational cost [45]. For both elements, the relative stability of the highly symmetric clusters with respect to M_4 increased when the spin–orbit effects were taken into account. For Sb clusters, the stabilizing effect of the spin–orbit interactions was fairly minor (less than 1 kJ/mol/atom), but in the case of bismuth including the spin–orbit effects had a major

stabilizing impact (5–6 kJ/mol/atom) on the clusters. The large impact of including spin–orbit effects for Bi clusters is in agreement with a previous study on the electronic structure of the group V tetramers, where the spin–orbit effects for bismuth were also found to be large in comparison with P–Sb [66]. To be in line with the main theme of the present study, we have focused only on polyhedral clusters of antimony and bismuth, but further studies on less symmetric clusters using the applied two-component procedure are expected to provide interesting insights into the cluster chemistry of the heavier group 15 elements.

3.4 Electronic structure trends

Analogously to the previously studied group 15 nanotubes [24], the metallic character of the group 15 fullerenes increases when moving down from P to Bi. However, all studied cages are still semiconducting, and the differences in the HOMO–LUMO gaps between the elements are not very large. The HOMO–LUMO gaps of three representative, large polyhedra are as follows. Tetrahedral M_{444} (9,1): P: 1.6 eV; As: 1.6 eV; Sb 1.3 eV; Bi: 0.9 eV. Octahedral M_{456} (7,1): P: 1.6 eV; As: 1.6 eV; Sb: 1.3 eV; Bi: 1.0 eV. Icosahedral M_{500} (5,0): P: 1.5 eV; As: 1.6 eV; Sb: 1.4 eV; Bi: 1.2 eV. The differences between the structural families are very small, the largest difference being 0.3 eV for the Bi tetrahedron and icosahedron. It should be noted that the pure BP86 density functional applied here underestimates the HOMO–LUMO gaps due to self-interaction error, as the B3LYP hybrid density functional has been shown to predict gaps close to 3.0 eV for large phosphorus tetrahedra such as P_{444} [3].

We investigated the electronic characteristics of the group 15 fullerenes in detail by means of density of states (DOS) analysis. The DOS analyses for the tetrahedral M_{84} cages are illustrated as a representative example in Fig. 6. In good agreement with the previous studies on group 15 bulk structures [6] and nanotubes, [24] the DOS plots in the Fig. 6 show the amount of s–p mixing to clearly decrease when moving down from P to Bi. In the case of phosphorus and arsenic, the DOS plots show s–p mixing in the valence region, especially in the s-dominated region (-20 to -12 eV), but also in the p-dominated region (-12 to -5 eV). However, for antimony, only minor s–p mixing is observed mainly within the s-dominated region (-16 to -10 eV), and in the case of bismuth, the mixing is almost absent. It has been suggested previously [6] that the s–p mixing is a significant contributing factor to the fact that in ambient pressures black phosphorus exists as orthorhombic-layered structure, while the heavier congeners adopt the rhombohedral structure. In this respect, the decreased s–p mixing might also play an important role in the structural chemistry of the polyhedral cages, making

the cages composed of heavier elements less strained due to more flexible pure p-type bonding.

4 Conclusions

The structural and electronic trends of polyhedral group 15 fullerenes were systematically investigated using quantum chemical methods. The structures and stabilities of the studied polyhedral cages were found to converge smoothly toward their experimentally known bulk counterparts, and they were also found to be thermodynamically stable with respect to the experimentally known tetra-atomic allotropes. Tetrahedral structures were found to be the thermodynamically most favorable, followed by octahedral and icosahedral structural families. The polyhedral cages can be further stabilized by stacking them into multilayered, bulk-like structures. The most notable periodic trends within the studied elements were the decreasing structural strain and decreasing amount of s–p mixing when moving down from P to Bi and the significant impact of the spin–orbit effects for the relative stability of the Bi cages. The obtained structural characteristics and periodic trends are expected to help in the experimental characterization of novel inorganic nanostructures composed of group 15 elements.

References

1. Tenne R, Seifert G (2009) Recent progress in the study of inorganic nanotubes and fullerene-like structures. Ann Rev Mater Res 39:387–413
2. Greenwood NN, Earnshaw A (1997) Chemistry of the elements. Butterworth-Heineman, Oxford
3. Karttunen AJ, Linnolahti M, Pakkanen TA (2008) Structural principles of polyhedral allotropes of phosphorus. ChemPhysChem 9:2550–2558
4. Pyykko P, Desclaux JP (1979) Relativity and the periodic system of elements. Acc Chem Res 12:276–281
5. Pyykko P (1988) Relativistic effects in structural chemistry. Chem Rev 88:563–594
6. Seo DK, Hoffmann R (1999) What determines the structures of the group 15 elements? J Solid State Chem 147:26–37
7. Keyes RW (1953) The electrical properties of black phosphorus. Phys Rev 92:580
8. Goodman NB, Ley L, Bullett DW (1983) Valence-band structures of phosphorus allotropes. Phys Rev B 27:7440
9. Gonze X, Michenaud J, Vigneron J (1990) First-principles study of As, Sb, and Bi electronic properties. Phys Rev B 41:11827
10. Pyykko P (1979) Interpretation of secondary periodicity in the periodic system. J Chem Res S380–S381
11. Bernhardt TM, Stegemann B, Kaiser B, Rademann K (2003) Crystalline structures of Sb4 molecules in antimony thin films. Angew Chem Int Ed 42:199–202
12. Haeser M, Schneider U, Ahlrichs R (1992) Clusters of phosphorus: a theoretical investigation. J Am Chem Soc 114:9551–9559
13. Han J, Morales JA (2004) A theoretical investigation on fullerene-like phosphorus clusters. Chem Phys Lett 396:27–33
14. Seifert G, Heine T, Fowler PW (2001) Inorganic nanotubes and fullerenes. Eur Phys J D At Mol Opt Plasma Phys 16:341–343
15. Moses MJ, Fettinger JC, Eichhorn BW (2003) Interpenetrating As-20 fullerene and Ni-12 icosahedra in the onion-skin [As@Ni-12@As-20](3−) ion. Science 300:778–780
16. Shen M, Schaefer HF III (1994) Dodecahedral and smaller arsenic clusters: As[sub n], n = 2, 4, 12, 20. J Chem Phys 101:2261–2266
17. Baruah T, Pederson MR, Zope RR, Beltrán MR (2004) Stability of Asn [n = 4, 8, 20, 28, 32, 36, 60] cage structures. Chem Phys Lett 387:476–480
18. Karttunen AJ, Linnolahti M, Pakkanen TA (2007) Icosahedral and ring-shaped allotropes of arsenic. ChemPhysChem 8:2373–2378
19. Nava P, Ahlrichs R (2008) Theoretical investigation of clusters of phosphorus and arsenic: fascination and temptation of high symmetries. Chem Eur J 14:4039–4045
20. Sattler K, Muehlbach J, Recknagel E (1980) Generation of metal clusters containing from 2 to 500 atoms. Phys Rev Lett 45:821
21. Karttunen AJ, Linnolahti M, Pakkanen TA (2007) Icosahedral and ring-shaped allotropes of phosphorus. Chem Eur J 13:5232–5237
22. Li SF, Gao L, Gong XG, Guo ZX (2008) No cage, no tube: relative stabilities of nanostructures. J Phys Chem C 112:13200–13203
23. Wahl B, Kloo L, Ruck M (2008) The molecular cluster [Bi10Au2](SbBi3Br9)2. Angew Chem Int Ed 47:3932–3935
24. Karttunen AJ, Tanskanen JT, Linnolahti M, Pakkanen TA (2009) Structural and electronic trends among group 15 elemental nanotubes. J Phys Chem C 113:12220–12224
25. Becke AD (1988) Density-functional exchange-energy approximation with correct asymptotic-behavior. Phys Rev A 38:3098–3100
26. Vosko SH, Wilk L, Nusair M (1980) Accurate spin-dependent electron liquid correlation energies for local spin-density calculations—a critical analysis. Can J Phys 58:1200–1211
27. Perdew JP (1986) Density-functional approximation for the correlation-energy of the inhomogeneous electron-gas. Phys Rev B 33:8822–8824
28. Schaefer A, Horn H, Ahlrichs R (1992) Fully optimized contracted Gaussian-basis sets for atoms Li to Kr. J Chem Phys 97:2571–2577
29. Weigend F, Ahlrichs R (2005) Balanced basis sets of split valence, triple zeta valence and quadruple zeta valence quality for H to Rn: design and assessment of accuracy. Phys Chem Chem Phys 7:3297–3305
30. Schafer A, Huber C, Ahlrichs R (1994) Fully optimized contracted Gaussian-basis sets of triple zeta valence quality for atoms Li to Kr. J Chem Phys 100:5829–5835
31. Metz B, Stoll H, Dolg M (2000) Small-core multiconfiguration-Dirac-Hartree-Fock-adjusted pseudopotentials for post-d main group elements: application to PbH and PbO. J Chem Phys 113:2563–2569
32. Eichkorn K, Treutler O, Oehm H, Haeser M, Ahlrichs R (1995) Auxiliary basis-sets to approximate coulomb potentials. Chem Phys Lett 240:283–289
33. Sierka M, Hogekamp A, Ahlrichs R (2003) Fast evaluation of the Coulomb potential for electron densities using multipole

accelerated resolution of identity approximation. J Chem Phys 118:9136–9148

34. Eichkorn K, Weigend F, Treutler O, Ahlrichs R (1997) Auxiliary basis sets for main row atoms and transition metals and their use to approximate Coulomb potentials. Theor Chem Acc 97:119–124

35. Weigend F (2006) Accurate Coulomb-fitting basis sets for H to Rn. Phys Chem Chem Phys 8:1057–1065

36. Weigend F, Haeser M (1997) RI-MP2: first derivatives and global consistency. Theor Chem Acc 97:331–340

37. Weigend F, Haeser M, Patzelt H, Ahlrichs R (1998) RI-MP2: optimized auxiliary basis sets and demonstration of efficiency. Chem Phys Lett 294:143–152

38. Hattig C, Weigend F (2000) CC2 excitation energy calculations on large molecules using the resolution of the identity approximation. J Chem Phys 113:5154–5161

39. Haettig C, Hellweg A, Koehn A (2006) Distributed memory parallel implementation of energies and gradients for second-order Moller-Plesset perturbation theory with the resolution-of-the-identity approximation. Phys Chem Chem Phys 8:1159–1169

40. Hellweg A, Haettig C, Hoefener S, Klopper W (2007) Optimized accurate auxiliary basis sets for RI-MP2 and RI-CC2 calculations for the atoms Rb to Rn. Theor Chem Acc 117:587–597

41. Woon DE, Dunning TH (1993) Gaussian-basis sets for use in correlated molecular calculations. 3. The atoms aluminum through argon. J Chem Phys 98:1358–1371

42. Wilson AK, Woon DE, Peterson KA, Dunning TH (1999) Gaussian basis sets for use in correlated molecular calculations. IX. The atoms gallium through krypton. J Chem Phys 110:7667–7676

43. Deglmann P, Furche F, Ahlrichs R (2002) An efficient implementation of second analytical derivatives for density functional methods. Chem Phys Lett 362:511–518

44. Ahlrichs R, Baer M, Haeser M, Horn H, Koelmel C (1989) Electronic-structure calculations on workstation computers—the program system turbomole. Chem Phys Lett 162:165–169

45. Armbruster MK, Weigend F, van Wuellen C, Klopper W (2008) Self-consistent treatment of spin-orbit interactions with efficient Hartree-Fock and density functional methods. Phys Chem Chem Phys 10:1748–1756

46. CFOUR, Coupled-Cluster techniques for Computational Chemistry, a quantum-chemical program package by J. F. Stanton, J. Gauss, M. E. Harding, P. G. Szalay with contributions from A. A. Auer, R. J. Bartlett, U. Benedikt, C. Berger, D. E. Bernholdt, Y. J. Bomble, L. Cheng, O. Christiansen, M. Heckert, O. Heun, C. Huber, T.-C. Jagau, D. Jonsson, J. Jusélius, K. Klein, W. J. Lauderdale, D. A. Matthews, T. Metzroth, D. P. O'Neill, D. R. Price, E. Prochnow, K. Ruud, F. Schiffmann, W. Schwalbach, S. Stopkowicz, A. Tajti, J. Vázquez, F. Wang, J. D. Watts and the integral packages MOLECULE (J. Almlöf and P. R. Taylor), PROPS (P. R. Taylor), ABACUS (T. Helgaker, H. J. Aa. Jensen, P. Jørgensen, and J. Olsen), and ECP routines by A. V. Mitin and C. van Wüllen. For the current version, see http://www.cfour.de

47. Harding ME, Metzroth T, Gauss J, Auer AA (2008) Parallel calculation of CCSD and CCSD(T) analytic first and second derivatives. J Chem Theory Comput 4:64–74

48. Chin Tang A, Qiang Huang F (1995) Stability rules of icosahedral (Ih or I) fullerenes. Chem Phys Lett 247:494–501

49. Tang AuChin, Huang FuQiang (1996) Electronic structures of octahedral fullerenes. Chem Phys Lett 263:733–741

50. Odom TW, Huang J, Kim P, Lieber CM (2000) Structure and electronic properties of carbon nanotubes. J Phys Chem B 104:2794–2809

51. Saunders M (1991) Buckminsterfullerane—the inside story. Science 253:330–331

52. Dodziuk H, Nowinski K (1996) 'Horror vacui' or topological in-out isomerism in perhydrogenated fullerenes: C60H60 and monoalkylated perhydrogenated fullerenes. Chem Phys Lett 249:406–412

53. Linnolahti M, Karttunen AJ, Pakkanen TA (2006) Remarkably stable icosahedral fulleranes: C80H80 and C180H180. ChemPhysChem 7:1661–1663

54. Linnolahti M, Kinnunen NM, Pakkanen TA (2006) Structural preferences of single-walled silica nanostructures: nanospheres and chemically stable nanotubes. Chem Eur J 12:218–224

55. Kraetschmer W, Lamb LD, Fostiropoulos K, Huffman DR (1990) Solid C60: a new form of carbon. Nature 347:354–358

56. Bulgakov AV, Bobrenok OF, Kosyakov VI (2000) Laser ablation synthesis of phosphorus clusters. Chem Phys Lett 320:19–25

57. Bulgakov AV, Bobrenok OF, Kosyakov VI, Ozerov I, Marine W, Heden M, Rohmund F, Campbell EEB (2002) Phosphorus clusters: synthesis in the gas-phase and possible cagelike and chain structures. Phys Solid State 44:617–622

58. Bulgakov AV, Bobrenok OF, Ozerov I, Marine W, Giorgio S, Lassesson A, Campbell EEB (2004) Phosphorus cluster production by laser ablation phosphorus cluster production by laser ablation. Appl Phys A Mater Sci Process 79:1369–1372

59. Sedo O, Vorac Z, Alberti M, Havel H (2004) Laser ablation synthesis of new phosphorus and phosphorus-sulfur clusters and their TOF mass spectrometric identification. Polyhedron 23:1199–1206

60. Špalt Z, Alberti M, Peña-Méndez E, Havel J (2005) Laser ablation generation of arsenic and arsenic sulfide clusters. Polyhedron 24:1417–1424

61. Derrouiche S, Loebick CZ, Pfefferle L (2010) Optimization of routes for the synthesis of bismuth nanotubes: implications for nanostructure form and selectivity. J Phys Chem C 114:3431–3440

62. Li L, Yang YW, Huang XH, Li GH, Ang R, Zhang LD (2006) Fabrication and electronic transport properties of Bi nanotube arrays. Appl Phys Lett 88:103119

63. Park C, Sohn H (2007) Black phosphorus and its composite for lithium rechargeable batteries. Adv Mater 19:2465–2468

64. Pfitzner A (2006) Phosphorus remains exciting!. Angew Chem Int Ed 45:699–700

65. Jayasekera B, Somaskandan K, Brock SL (2004) Liberation of pnicogen chains from $Cu_2P_{1.8}As_{1.2}I_2$: synthesis and characterization of a new allotrope of P–As. Inorg Chem 43:6902–6904

66. Zhang H, Balasubramanian K (1992) Electronic structure of the group V tetramers (P4–Bi4). J Chem Phys 97:3437